

---

---

# Visual Assessment Versus Quantitative Assessment of $^{11}\text{C}$ -PIB PET and $^{18}\text{F}$ -FDG PET for Detection of Alzheimer's Disease

Steven Ng<sup>1</sup>, Victor L. Villemagne<sup>1-3</sup>, Sam Berlangieri<sup>1</sup>, Sze-Ting Lee<sup>1</sup>, Martin Cherk<sup>1</sup>, Sylvia J. Gong<sup>1</sup>, Uwe Ackermann<sup>1</sup>, Tim Saunderson<sup>1</sup>, Henri Tochon-Danguy<sup>1</sup>, Gareth Jones<sup>1</sup>, Clare Smith<sup>1</sup>, Graeme O'Keefe<sup>1</sup>, Colin L. Masters<sup>2,3</sup>, and Christopher C. Rowe<sup>1</sup>

<sup>1</sup>Department of Nuclear Medicine, Centre for PET, Austin Health, Heidelberg, Victoria, Australia; <sup>2</sup>Department of Pathology, University of Melbourne, Parkville, Victoria, Australia; and <sup>3</sup>The Mental Health Research Institute of Victoria, Parkville, Victoria, Australia

---

Amyloid- $\beta$  (A $\beta$ ) imaging with *N*-methyl- $^{11}\text{C}$ -2-(4'-methylamino-phenyl)-6-hydroxy-benzothiazole ( $^{11}\text{C}$ -6-OH-BTA-1; also known as  $^{11}\text{C}$ -PIB) shows a robust increase in cortical binding in Alzheimer's disease (AD). The aim of this study was to explore the clinical potential of A $\beta$  imaging for the diagnosis of AD by comparison of the accuracy of visual reading of  $^{11}\text{C}$ -PIB images with quantitative analysis and  $^{18}\text{F}$ -FDG. **Methods:** Fifteen AD patients (age,  $71.1 \pm 11.3$  y [mean  $\pm$  SD]; mini-mental state examination [MMSE],  $18.9 \pm 9.3$  [mean  $\pm$  SD]) and 25 healthy control (HC) subjects (age,  $71.9 \pm 6.82$  y; MMSE  $\geq 28$ ) underwent 90-min dynamic  $^{11}\text{C}$ -PIB PET and 20-min static  $^{18}\text{F}$ -FDG PET.  $^{11}\text{C}$ -PIB images, generated from data acquired between 40 and 70 min after injection, and  $^{18}\text{F}$ -FDG images were rated separately by 2 readers as normal, possible AD, or probable AD. Quantitative analyses used the distribution volume ratio (DVR) of frontal cortex, parietotemporal cortex, posterior cingulate, and caudate nucleus for  $^{11}\text{C}$ -PIB and standardized uptake value ratio (SUVR) of parietotemporal cortex and posterior cingulate for  $^{18}\text{F}$ -FDG, using cerebellar cortex as the reference region. Receiver-operating-characteristic (ROC) analysis was performed to compare the accuracy of quantitative measures. To determine the effect of age on diagnostic accuracy, the median age of the AD subjects (74 y) was chosen to separate the cohort into younger ( $64.4 \pm 5.8$  y) and older ( $78.6 \pm 4.1$  y) groups. **Results:** Visual agreement between readers was excellent for  $^{11}\text{C}$ -PIB ( $\kappa = 0.90$ ) and good for  $^{18}\text{F}$ -FDG ( $\kappa = 0.56$ ).  $^{11}\text{C}$ -PIB was more accurate than  $^{18}\text{F}$ -FDG both on visual reading (accuracy, 90% vs. 70%,  $P = 0.05$ ) and ROC analysis (95% vs. 83%,  $P = 0.02$ ). Accuracy declined more with  $^{18}\text{F}$ -FDG than with  $^{11}\text{C}$ -PIB in the older group. **Conclusion:** Visual analysis of  $^{11}\text{C}$ -PIB images appears more accurate than visual reading of  $^{18}\text{F}$ -FDG for identification of AD and has accuracy similar to quantitative analysis of a 90-min dynamic scan. The accuracy of  $^{11}\text{C}$ -PIB PET is limited by cortical binding in some healthy elderly subjects, consistent with postmortem studies of cerebral A $\beta$ . Longitudinal follow-up is required to determine if this represents detection of preclinical AD.

**Key Words:** Alzheimer's disease; amyloid- $\beta$ ;  $^{11}\text{C}$ -PIB; PET;  $^{18}\text{F}$ -FDG; brain imaging

**J Nucl Med 2007; 48:547-552**

DOI: 10.2967/jnumed.106.037762

---

**F**or more than a decade,  $^{18}\text{F}$ -FDG PET has been used to assist the diagnosis of Alzheimer's disease (AD). Temporoparietal and posterior cingulate hypometabolism with sparing of subcortical structures and sensorimotor and occipital cortices are characteristic of AD (1). Both visual interpretation and quantitative diagnostic approaches yield a similar sensitivity of approximately 85%–95%, and specificity ranging from 70% to 90%, in diagnosing AD (1–4). Accuracy is influenced by disease severity and subject age, as the degree of hypometabolism is proportional to the degree of cognitive impairment (5), and the characteristic pattern of AD is less apparent in older patients (5–8). Age-related atrophy and more frequent multiple pathology contributing to the dementia make visual diagnosis of  $^{18}\text{F}$ -FDG PET images more difficult in the elderly.

Amyloid- $\beta$  (A $\beta$ ) plaques are one of the pathologic hallmarks of AD. Extensive cortical plaques are present in patients with AD at postmortem, and A $\beta$  deposition is believed to begin well before the onset of symptoms (9,10). Recently, a  $^{11}\text{C}$ -labeled derivative of the thioflavin-T amyloid dye was shown to be suitable for in vivo quantification of cerebral A $\beta$  (11). *N*-Methyl- $^{11}\text{C}$ -2-(4'-methylamino-phenyl)-6-hydroxy-benzothiazole ( $^{11}\text{C}$ -6-OH-BTA-1; also known as "Pittsburgh Compound-B" or  $^{11}\text{C}$ -PIB) has been shown in vitro to possess high affinity (dissociation constant, 1–2 nM) and high specificity for A $\beta$  fibrils and bind to A $\beta$  plaques but not neurofibrillary tangles in postmortem human brain homogenates (12,13). Quantification of  $^{11}\text{C}$ -PIB PET has shown a robust difference in cortical binding between AD and age-matched healthy control (HC) subjects, while showing minimal retention in cerebellum (11), a region

---

Received Nov. 1, 2006; revision accepted Jan. 20, 2007.

For correspondence contact: Christopher C. Rowe, MD, Department of Nuclear Medicine, Centre for PET, Austin Health, 145 Studley Rd., Heidelberg, Victoria 3084, Australia.

E-mail: christopher.rowe@austin.org.au

known to be relatively devoid of neuritic A $\beta$  plaque (14,15).

A $\beta$  imaging with  $^{11}\text{C}$ -PIB provides researchers and clinicians the opportunity to assess A $\beta$  burden in vivo.  $^{11}\text{C}$ -PIB imaging has great potential as a diagnostic tool and as a surrogate measure of response to anti-amyloid therapy. Although visual interpretation of  $^{11}\text{C}$ -PIB PET scans would seem to be the most expedient method for diagnosis of AD in clinical practice, all studies reported to date have relied on more complex quantitative techniques. The most widely used quantitative method has been graphical analysis by Logan plot of a 60- or 90-min dynamic scan using the cerebellar cortex as the reference region to derive the distribution volume ratio (DVR) (11,16) or binding potential (i.e., DVR - 1) (17). To our knowledge, the accuracy of visual analysis of  $^{11}\text{C}$ -PIB PET images has not been reported nor has it been compared with  $^{18}\text{F}$ -FDG PET.

The purpose of the study was to determine the accuracy of visual interpretation of  $^{11}\text{C}$ -PIB PET images for differentiating AD from age-matched HC subjects and to compare this to (a) visual interpretation of  $^{18}\text{F}$ -FDG PET images in the same subjects, (b) quantitative measurement of  $^{11}\text{C}$ -PIB binding, and (c) quantitative measurement of regional cerebral  $^{18}\text{F}$ -FDG uptake.

## MATERIALS AND METHODS

### Subjects

Twenty-five HC subjects were recruited through the Healthy Aging Study of the Mental Health Research Institute, Victoria, and had normal cognitive function on neuropsychologic assessment. Fifteen AD patients were recruited through the Austin Hospital Memory Disorders Clinic. All subjects fulfilled National Institute of Neurological and Communicative Diseases and Stroke/Alzheimer's Disease and Related Disorders Association criteria for probable AD (18). None of the subjects had diagnostic features of dementia with Lewy bodies, frontotemporal dementia, or other non-AD dementias. Most AD subjects had mild-to-moderate dementia, with two thirds scoring >20 on the mini-mental state examination (MMSE). Table 1 provides the demographic details of the subjects. Informed consent was obtained from each subject, or their next of kin, and all procedures were approved by the Austin Health Human Research Ethics Committee.

### Tracer Synthesis

Production of  $^{11}\text{C}$ -PIB was performed in the Department of Nuclear Medicine and Centre for PET, Austin Hospital, using the 1-step  $^{11}\text{C}$ -methyl triflate approach (19). The average radiochemical yield was 20% after a synthesis time of 45 min, with a radiochemical purity of >98%.

### Image Acquisition Protocols

T1-weighted 3-dimensional spoiled gradient recalled MRI was obtained for all subjects for PET image coregistration and to facilitate anatomic localization of regions of interest (ROIs) used in the analysis of the PET data. The MR images were also screened for non-AD pathology, such as stroke and tumor.

All PET brain images were acquired using a Philips ADAC Allegro full-ring 3-dimensional PET system with PIXELAR germanium oxyorthosilicate crystal detectors. The system has a spatial resolution of approximately 4.4 mm (full width at half maximum) in the center of the field of view. A short transmission scan (75 s) was first acquired using  $^{137}\text{Cs}$  transmission source for validation of correct head positioning and for nonuniform attenuation and scatter correction of the emission scan; this was followed by a 90-min emission scan performed in list-mode from the time of intravenous injection of 370 MBq of  $^{11}\text{C}$ -PIB. The emission sinograms were sorted from the list-mode raw data into 28 dynamic frames (4  $\times$  30 s, 9  $\times$  60 s, 3  $\times$  90 s, 10  $\times$  360 s, and 2  $\times$  600 s). All dynamic images were reconstructed from the dead-time and decay-corrected dynamic emission sinograms using the row-action maximum likelihood algorithm (20) with the optimal iteration number of 1, relaxation of 0.006, and blob radius of 2.5.

On completion of  $^{11}\text{C}$ -PIB image acquisition, the subjects were injected intravenously with 250 MBq of  $^{18}\text{F}$ -FDG and remained in a darkened, quiet room. All subjects fasted for at least 6 h and were normoglycemic at the time of  $^{18}\text{F}$ -FDG injection. A 20-min static PET emission scan was acquired 60 min after injection of  $^{18}\text{F}$ -FDG on the same camera, and images were reconstructed using the same image reconstruction techniques.

### Data Analysis

Coregistration of the PET images with the MRI was performed with statistical parametric mapping 2 (SPM2; Wellcome Department of Cognitive Neurology, London, U.K.). Mean radioactivity values were obtained from ROIs for cortical, subcortical, and cerebellar regions, and decay-corrected time-activity curves were generated.

Plots of the time course of ROI-to-cerebellum ratios showed that apparent steady state between the different brain regions and

**TABLE 1**  
Demographic Details

Group	No. of subjects	M/F	Age* (y)	MMSE*	CDR*
AD	Total = 15	7/8	71.1 $\pm$ 11.3	18.9 $\pm$ 9.3	1.3 $\pm$ 0.7
	Age < 74 y = 7	5/2	61 $\pm$ 4.6	17.7 $\pm$ 9.9	1.3 $\pm$ 0.7
	Age $\geq$ 74 y = 8	2/6	81.1 $\pm$ 4.4	20 $\pm$ 0.9	1.3 $\pm$ 0.8
HC	Total = 25	14/11	71.9 $\pm$ 6.8	29.2 $\pm$ 0.9	0.1 $\pm$ 0.2
	Age < 74 = 12	8/4	66.3 $\pm$ 5.1	29.4 $\pm$ 0.8	0
	Age $\geq$ 74 = 13	6/7	77 $\pm$ 3.6	29.1 $\pm$ 1.0	0.12 $\pm$ 0.22

\*Mean  $\pm$  SD.

CDR = clinical dementia rating.

cerebellum, a region relatively unaffected by A $\beta$  deposition, was attained after 40 min after  $^{11}\text{C}$ -PIB injection. Therefore, summed images of SUV data acquired from 40 to 70 min after injection were generated for visual analysis.

$^{11}\text{C}$ -PIB and  $^{18}\text{F}$ -FDG images were read separately by a nuclear medicine physician with expertise in neuroimaging, who has read >1,000  $^{18}\text{F}$ -FDG brain PET studies (reader A), and a recently qualified nuclear medicine specialist, who has read between 50 and 100  $^{18}\text{F}$ -FDG brain PET scans (reader B). Both were unaware of the clinical diagnosis.  $^{11}\text{C}$ -PIB and  $^{18}\text{F}$ -FDG images were presented separately and randomly. Images were graded as normal, possible AD, or probable AD. Neither of the readers had prior experience with  $^{11}\text{C}$ -PIB PET. Transverse, sagittal, and coronal views were available for viewing using standard MedImage MedView or Philips Syntegra software. Before reading the  $^{11}\text{C}$ -PIB images, a demonstration was given using 2 AD images and 1 typical HC  $^{11}\text{C}$ -PIB image (Fig. 1) from subjects not included in this study cohort. Readers were advised to use a rainbow color scale normalized by setting cerebellar white matter to yellow. Subjects with cortical binding (yellow or red) in frontal, posterior cingulate, precuneus, parietal cortex, and temporal cortex were classified as having possible or probable AD, depending on intensity and extent of uptake.  $^{18}\text{F}$ -FDG images were read with the same image display software, but the readers were able to use the color scale and criteria they preferred for routine clinical brain  $^{18}\text{F}$ -FDG PET reporting.

SPM was used to identify key areas for subsequent quantitative analysis. Six AD and 6 HC  $^{11}\text{C}$ -PIB studies were randomly selected. These were coregistered to the subjects' MRI using SPM2 and then normalized to a standardized template (Montreal Neurological Institute, McGill University, Canada). Two sample  $t$  tests were performed, using SPM2, to identify regions that showed the greatest difference in AD from HC (i.e., regions above a threshold of corrected  $P$  value < 0.01) (Fig. 2). The 5 key areas identified were the medial orbitofrontal, precuneus/posterior cingulate, caudate nucleus, lateral temporal, and parietal gray matter.

To quantify  $^{11}\text{C}$ -PIB uptake in the regions identified on SPM analysis, ROIs were drawn manually by an experienced nuclear medicine physician onto the coregistered MR image, which were subsequently transferred to the corresponding PET images. Each

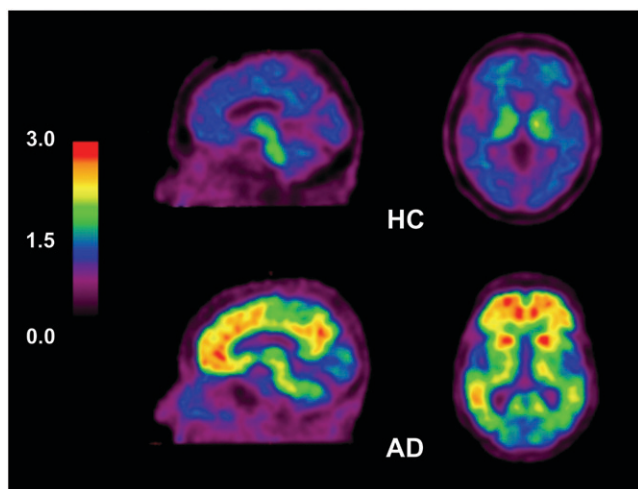


**FIGURE 1.**  $^{11}\text{C}$ -PIB PET images show white matter uptake of  $^{11}\text{C}$ -PIB in HC subject (top) and extensive cortical and subcortical uptake in AD patient (bottom). Note relative sparing of sensorimotor and occipital cortex in AD patient.

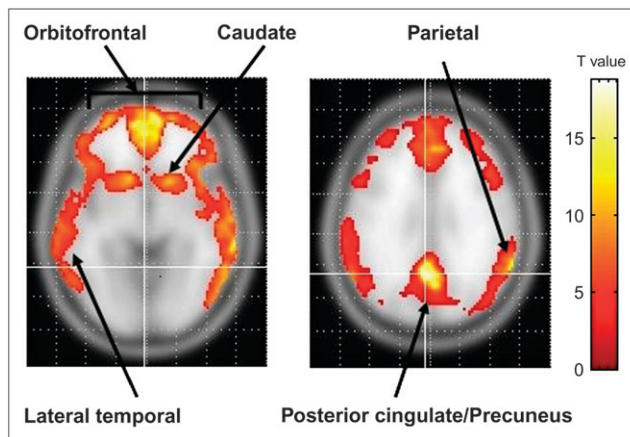


**FIGURE 2.** SPM analysis of AD vs. HC subjects. Results are superimposed on transverse T1-weighted MRI brain templates at level of caudate nucleus (left) and at level of posterior cingulate cortex (right). Highlighted areas represent brain regions where AD had significantly higher  $^{11}\text{C}$ -PIB uptake than HC. Five regions (indicated by arrows) are clearly identified (height threshold, uncorrected  $P = 0.01$ ; voxel extension, 125).

region was drawn symmetrically on both cerebral hemispheres to obtain an average uptake value. Care was taken to avoid white matter. The regional DVRs were determined through graphical analysis. To avoid arterial blood sampling, a simplified approach was applied using the cerebellar cortex as the input function. (14,21). The DVR is the slope of the linear section of the plot of:

$$\int_0^T C_{Tissue}(t)dt / C_{Tissue}(T) \text{ versus } \int_0^T C_{Cb}(t)dt / C_{Tissue}(T),$$

where  $C_{Tissue}$  is the decay-corrected PET radioactivity concentration in brain regions and  $C_{Cb}$  is the decay-corrected PET radioactivity concentration in the cerebellar cortex.

The mean of the DVRs for the above ROIs was calculated for each subject's  $^{11}\text{C}$ -PIB scan and termed "mean regional DVR" (mrDVR) for subsequent statistical analysis.

For quantification of  $^{18}\text{F}$ -FDG PET, the same coregistration method was applied. In contrast to  $^{11}\text{C}$ -PIB analysis, only lateral temporal, parietal, and posterior cingulate cortices were used as the ROI. A mean standardized uptake value (SUV) of these 3 regions was obtained, which was subsequently normalized to the SUV of the cerebellar cortex to obtain the mean regional SUV ratio (mrSUVr) for further statistical analysis.

### Statistical Analysis

$\kappa$ -Statistics were calculated to assess the interobserver agreement for the visual interpretation of both  $^{11}\text{C}$ -PIB and  $^{18}\text{F}$ -FDG images.

For the assessment of the accuracy of visual interpretation of  $^{11}\text{C}$ -PIB PET in differentiating AD (both possible and probable AD) from HC,  $2 \times 2$  contingency analysis was used to determine the test sensitivity and specificity. Diagnostic accuracy of  $^{18}\text{F}$ -FDG PET was also determined with the same method and compared with the  $^{11}\text{C}$ -PIB results.

Receiver-operating-characteristic (ROC) curves were generated using a nonparametric approach to assess the accuracy of the mrDVR and mrSUVr for AD diagnosis. Cutoff values that produced the highest test sensitivity and specificity were determined by the maximum area under curve (AUC).

Cohen's effect size was calculated as the difference in mean DVR (for  $^{11}\text{C}$ -PIB), and mean SUVR (for  $^{18}\text{F}$ -FDG), of AD and HC divided by the pooled SD.

To assess the effect of age on diagnostic accuracy, the cohort was separated according to the median age of the AD cohort into 2 groups, younger (<74 y) and older ( $\geq 74$  y), and the above analyses were performed on both categories.

## RESULTS

### Visual Analysis

Results of the visual analysis are summarized in Table 2. Agreement between readers A and B for the diagnosis of AD by visual assessment was excellent for  $^{11}\text{C}$ -PIB ( $\kappa = 0.90$ ) and good for  $^{18}\text{F}$ -FDG ( $\kappa = 0.56$ ).

There was greater certainty in interpretation of  $^{11}\text{C}$ -PIB images than  $^{18}\text{F}$ -FDG images, with fewer subjects classified as having possible AD. Between the 2 readers, 8  $^{11}\text{C}$ -PIB images (10%) were classified as possible AD, whereas 18  $^{18}\text{F}$ -FDG images (23%) were classified as possible AD. Both readers classified correctly all 15 AD subjects as probable AD on  $^{11}\text{C}$ -PIB images.

The test sensitivity, specificity, and accuracy of visual interpretation of  $^{11}\text{C}$ -PIB and  $^{18}\text{F}$ -FDG are summarized in Table 3.  $^{11}\text{C}$ -PIB scans appeared to be more accurate ( $\sim 90\%$ ) than  $^{18}\text{F}$ -FDG scans ( $\sim 70\%$ ). Such difference was significant in reader B ( $P = 0.03$ ) but just failed to reach significance in reader A ( $P = 0.06$ ). Age appeared to have an impact on specificity but not on sensitivity in  $^{11}\text{C}$ -PIB. For  $^{18}\text{F}$ -FDG scans, a reduction in both test sensitivity and specificity was observed in the older group when compared with the younger subjects. This was particularly evident for the more experienced reader (A), whose accuracy declined from 95% in the younger group to 57% in the older group ( $P < 0.01$ ).

### Quantitative Analysis

The mrDVR and mrSUVR values are shown in Figures 3 and 4, respectively. The mrDVR of the AD group was significantly higher than that of the HC group. Three HC subjects had DVRs close to the range of AD. Although the mean of mrSUVR was significantly higher in HC than AD

**TABLE 3**  
Comparison of Accuracy of  $^{11}\text{C}$ -PIB vs.  $^{18}\text{F}$ -FDG  
(Visual Analysis)

Comparison	Sensitivity	Specificity	Accuracy
<b>Reader A</b>			
$^{11}\text{C}$ -PIB	1.00	0.88	0.93*
$^{18}\text{F}$ -FDG	0.73	0.76	0.75*
<b>Reader B</b>			
$^{11}\text{C}$ -PIB	1.00	0.80	0.88†
$^{18}\text{F}$ -FDG	0.86	0.56	0.68†
<b>Young vs. old‡</b>			
$^{11}\text{C}$ -PIB < 74	1.00	0.96	0.97
$^{11}\text{C}$ -PIB $\geq 74$	1.00	0.73	0.83
$^{18}\text{F}$ -FDG < 74	1.00§	0.75	0.84
$^{18}\text{F}$ -FDG $\geq 74$	0.63§	0.58	0.60

\* $P < 0.06$ .

† $P < 0.03$ .

‡Mean results of reader A and reader B.

§ $P < 0.01$ .

subjects, the difference in mrSUVR appeared to be less robust than the difference observed in mrDVR of  $^{11}\text{C}$ -PIB scans. The Cohen's effect size for  $^{11}\text{C}$ -PIB was 3.87 and for  $^{18}\text{F}$ -FDG was 1.53.

ROC analysis of mrDVR showed that quantitative  $^{11}\text{C}$ -PIB analysis was 95% accurate in AD diagnosis (Table 4), a result similar to visual analysis ( $\sim 90\%$ ) and significantly better than the mrSUVR of  $^{18}\text{F}$ -FDG scans ( $P = 0.02$ ).

Comparing ROC curves of the younger and the older groups revealed no difference in diagnostic accuracy in the  $^{11}\text{C}$ -PIB quantitative analysis, whereas a significant improvement (27% increase in AUC) was observed in the younger group for the  $^{18}\text{F}$ -FDG scans. AUCs for both  $^{11}\text{C}$ -PIB subgroups were 1.00, whereas AUCs for the  $^{18}\text{F}$ -FDG younger group versus the older group were 0.99 versus 0.73 ( $P = 0.02$ ).

**TABLE 2**  
Summary of Results of Visual Analysis Obtained from Both  
Readers (15 AD and 25 HC Subjects)

Comparison	Clinical diagnosis			
	Reader A		Reader B	
	AD	HC	AD	HC
<b><math>^{11}\text{C}</math>-PIB</b>				
Probable	15	0	15	0
Possible	0	3	0	5
Normal	0	22	0	20
<b><math>^{18}\text{F}</math>-FDG</b>				
Probable	10	1	11	1
Possible	1	5	2	10
Normal	4	19	2	14

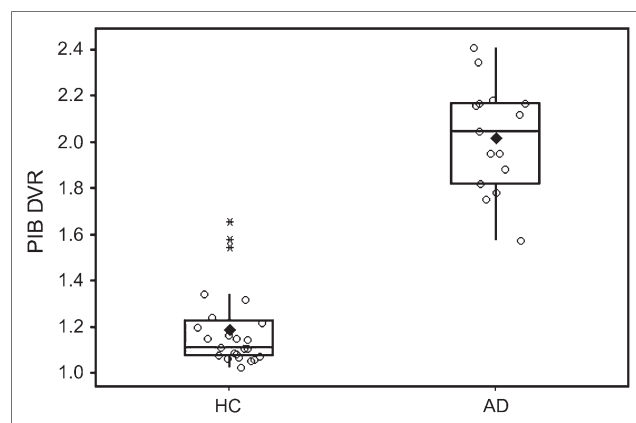


**FIGURE 3.** Box plot of  $^{11}\text{C}$ -PIB mrDVR of HC and AD shows median value, quartiles, outliers (\*), and mean (◆). Mean mrDVR (HC) =  $1.19 \pm 0.17$  vs. mean mrDVR (AD) =  $2.02 \pm 0.23$  ( $P < 0.01$ ; Cohen's effect size = 3.87 indicates nonoverlap of 97% in 2 distributions).

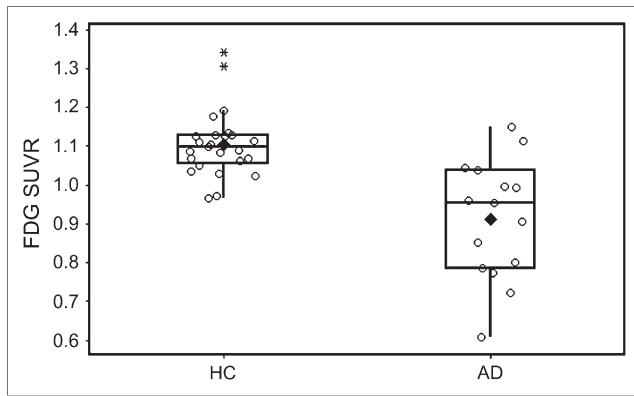


**FIGURE 4.** Box plot of  $^{18}\text{F}$ -FDG mrSUVR of HC and AD shows median value, quartiles, outliers (\*), and mean ( $\blacklozenge$ ). Mean mrSUVR (HC) =  $1.10 \pm 0.09$  vs. mean mrSUVR (AD) =  $0.91 \pm 0.15$  ( $P < 0.01$ ; Cohen's effect size = 1.53 indicates nonoverlap of 71% in 2 distributions).

## DISCUSSION

This study showed that imaging of specific disease-related pathology with the brain  $\text{A}\beta$  PET tracer  $^{11}\text{C}$  PIB may provide diagnostic advantages over nonspecific measures such as hypometabolism on  $^{18}\text{F}$ -FDG PET. A similar advantage has recently been reported for a PET ligand with affinity to brain  $\text{A}\beta$  and  $\tau$  that differentiated HC subjects, subjects with mild cognitive impairment, and subjects with AD better than did  $^{18}\text{F}$ -FDG PET or volume on MRI (22). Our study also demonstrated that visual interpretation of a 30-min  $^{11}\text{C}$ -PIB PET image was as accurate as quantitative analysis of a 90-min dynamic scan and appropriate for routine clinical practice.  $^{11}\text{C}$ -PIB scans were easy to read after minimal training and were read with very high interobserver agreement and with accuracy exceeding 90%. Interobserver agreement was higher than that for  $^{18}\text{F}$ -FDG PET and readers were more confident with  $^{11}\text{C}$ -PIB images, classifying less as possible AD. Quantitative  $^{11}\text{C}$ -PIB analysis also demonstrated a diagnostic advantage over quantitative  $^{18}\text{F}$ -FDG PET, as reflected by the Cohen's effect size ( $^{11}\text{C}$ -PIB = 3.87 vs.  $^{18}\text{F}$ -FDG = 1.53) and a significant difference with ROC analysis (AUC, 100% vs. 87%).

The 5 regions used in our  $^{11}\text{C}$ -PIB quantitative analyses are areas known to have large deposits of  $\text{A}\beta$  plaques in AD (23,24). Autopsy series have shown up to 4-fold greater  $\text{A}\beta$

plaque density in frontal cortex than that in the mesial temporal region in early AD (10,25), whereas the visual cortex and primary sensorimotor cortex are not usually involved until very late in the disease course (23).

The 3 regions used in our quantitative  $^{18}\text{F}$ -FDG analysis have been shown consistently in previous literature to be the areas most affected metabolically in AD (3,26,27). Although there is no consensus on the most suitable reference region for normalization of SUVs for intersubject comparison of  $^{18}\text{F}$ -FDG scans, the cerebellar cortex has been widely utilized. The metabolism of cerebellar cortex has been shown to be relatively unaffected in mild-to-moderate AD (1,28,29), though significant hypometabolism has been reported in severe AD (30).

The accuracy of visual and quantitative analysis of  $^{18}\text{F}$ -FDG PET declined markedly in the older subjects. In the younger cohort with a mean age of 64 y, the sensitivity of  $^{18}\text{F}$ -FDG PET was 100%, with a specificity of 75%, producing an accuracy of 84%. In this group, the experienced reader had 95% accuracy. These figures accord with a recent metaanalysis of  $^{18}\text{F}$ -FDG PET for the diagnosis of AD that calculated pooled sensitivity and specificity estimates of 86% (4). The studies in the metaanalysis had mean subject ages ranging from early to late 60s. The few studies that have looked specifically at late-onset AD, defined as onset after the age of 65 y, have reported 20% lower accuracy in late-onset AD compared with early-onset AD for diagnosis based on visual or quantitative  $^{18}\text{F}$ -FDG PET findings (6,8,31,32). Our older AD group had a mean age of 81 y and, to our knowledge, there are no reports on the accuracy of  $^{18}\text{F}$ -FDG PET in a population of this age. The prevalence of AD at age 60 y is 1% but by age 85 y it is 25%. As the population ages, most patients presenting for diagnosis of AD will be  $>70$  y of age, presenting a challenge for  $^{18}\text{F}$ -FDG PET. More studies are needed to determine the accuracy of  $^{18}\text{F}$ -FDG PET in older subjects with AD. The accuracy of  $^{11}\text{C}$ -PIB PET was less affected by age. Sensitivity remained 100%, but specificity fell due to a higher number of positive scans in the older group of normal subjects whose mean age was 77 y. This is to be expected given that postmortem data show that  $\text{A}\beta$  plaque is present in 30% of the nondemented elderly population above 75 y of age (33,34). The number of "false-positive"  $^{11}\text{C}$ -PIB scans (27%) in our older cohort (age  $\geq 74$  y) is

**TABLE 4**  
Accuracy of  $^{11}\text{C}$ -PIB mrDVR and  $^{18}\text{F}$ -FDG mrSUVR by ROC Analysis

	Cutoff	SD*	Sensitivity	Specificity	Accuracy	AUC† (95% CI)
$^{11}\text{C}$ -PIB	1.54	2.0	1.00	0.92	0.95‡	0.995 (0.98–1.01)
$^{18}\text{F}$ -FDG	1.04	0.8	0.80	0.87	0.83	0.867 (0.73–0.96)

\*Number of SD away from the mean of HC.

†Significant difference in AUC ( $P = 0.02$ ).

‡No statistical significance when compared with global visual analysis.

CI = confidence interval for AUC.

consistent with this figure. Positive  $^{11}\text{C}$ -PIB scans in apparently normal elderly individuals have also been reported in 3 of 20 subjects over 65 y of age (35). Cerebrospinal fluid  $\text{A}\beta_{42}$  depressed to levels usually found in AD has been reported in healthy subjects with positive  $^{11}\text{C}$ -PIB scans (17). These elderly subjects with  $\text{A}\beta$  plaques may represent preclinical AD, as postmortem evidence suggests that  $\text{A}\beta$  deposition may begin up to 10 y before the onset of AD symptoms (9,10). Longitudinal follow-up is required to establish if this is the case. If so, the true accuracy of  $^{11}\text{C}$ -PIB PET for the detection of AD may be even greater than the 95% found in this study.

## CONCLUSION

$^{11}\text{C}$ -PIB PET shows great promise as an aid for the diagnosis of AD.  $^{11}\text{C}$ -PIB PET images appear easier to read and more accurate than  $^{18}\text{F}$ -FDG PET images in AD diagnosis, particularly in older subjects. The accuracy of visual analysis is comparable with the most widely utilized quantitative method of  $^{11}\text{C}$ -PIB image analysis.

## ACKNOWLEDGMENTS

This research was supported in part by funds from the Austin Hospital Medical Research Foundation, Neurosciences Victoria, the University of Melbourne, and the Department of Health and Ageing Commonwealth Government of Australia. We thank Jessica Sagona, Kunthi Pathmaraj, Bridget Chappell, Jason Bradley, and Gareth Jones for their crucial role during PET examinations and image processing.

## REFERENCES

- Herholz K, Salmon E, Perani D, et al. Discrimination between Alzheimer dementia and controls by automated analysis of multicenter FDG PET. *Neuroimage*. 2002;17:302–316.
- Silverman DH, Small GW, Chang CY, et al. Positron emission tomography in evaluation of dementia: regional brain metabolism and long-term outcome. *JAMA*. 2001;286:2120–2127.
- Silverman DH. Brain  $^{18}\text{F}$ -FDG PET in the diagnosis of neurodegenerative dementias: comparison with perfusion SPECT and with clinical evaluations lacking nuclear imaging. *J Nucl Med*. 2004;45:594–607.
- Patwardhan MB, McCrory DC, Matchar DB, Samsa GP, Rutschmann OT. Alzheimer disease: operating characteristics of PET: a meta-analysis. *Radiology*. 2004;231:73–80.
- Herholz K. FDG PET and differential diagnosis of dementia. *Alzheimer Dis Assoc Disord*. 1995;9:6–16.
- Sakamoto S, Ishii K, Sasaki M, et al. Differences in cerebral metabolic impairment between early and late onset types of Alzheimer's disease. *J Neurol Sci*. 2002;200:27–32.
- Yasuno F, Imamura T, Hirano N, et al. Age at onset and regional cerebral glucose metabolism in Alzheimer's disease. *Dement Geriatr Cogn Disord*. 1998;9:63–67.
- Mielke R, Herholz K, Grond M, Kessler J, Heiss WD. Differences of regional cerebral glucose metabolism between presenile and senile dementia of Alzheimer type. *Neurobiol Aging*. 1992;13:93–98.
- Hulette CM, Welsh-Bohmer KA, Murray MG, Saunders AM, Mash DC, McIntyre LM. Neuropathological and neuropsychological changes in "normal" aging: evidence for preclinical Alzheimer disease in cognitively normal individuals. *J Neuropathol Exp Neurol*. 1998;57:1168–1174.
- Morris JC, Price AL. Pathologic correlates of nondemented aging, mild cognitive impairment, and early-stage Alzheimer's disease. *J Mol Neurosci*. 2001;17:101–118.

- Klunk WE, Engler H, Nordberg A, et al. Imaging brain amyloid in Alzheimer's disease with Pittsburgh Compound-B. *Ann Neurol*. 2004;55:306–319.
- Mathis CA, Bacskai BJ, Kajdasz ST, et al. A lipophilic thioflavin-T derivative for positron emission tomography (PET) imaging of amyloid in brain. *Bioorg Med Chem Lett*. 2002;12:295–298.
- Klunk WE, Wang Y, Huang GF, Debnath ML, Holt DP, Mathis CA. Uncharged thioflavin-T derivatives bind to amyloid-beta protein with high affinity and readily enter the brain. *Life Sci*. 2001;69:1471–1484.
- Price JC, Klunk WE, Lopresti BJ, et al. Kinetic modeling of amyloid binding in humans using PET imaging and Pittsburgh Compound-B. *J Cereb Blood Flow Metab*. 2005;25:1528–1547.
- Verhoeff NP, Wilson AA, Takeshita S, et al. In-vivo imaging of Alzheimer disease beta-amyloid with [ $^{11}\text{C}$ ]JSB-13 PET. *Am J Geriatr Psychiatry*. 2004;12:584–595.
- Lopresti BJ, Klunk WE, Mathis CA, et al. Simplified quantification of Pittsburgh Compound B amyloid imaging PET studies: a comparative analysis. *J Nucl Med*. 2005;46:1959–1972.
- Fagan AM, Mintun MA, Mach RH, et al. Inverse relation between in vivo amyloid imaging load and cerebrospinal fluid Abeta(42) in humans. *Ann Neurol*. 2006;59:512–519.
- McKhann G, Drachman D, Folstein M, Katzman R, Price D, Stadlan EM. Clinical diagnosis of Alzheimer's disease: report of the NINCDS-ADRDA Work Group under the auspices of Department of Health and Human Services Task Force on Alzheimer's Disease. *Neurology*. 1984;34:939–944.
- Wilson AA, Meyer JH, Houle S, et al. A rapid one-step radiosynthesis of the beta-amyloid imaging radiotracer N-methyl-[( $^{11}\text{C}$ )2-(4'-methylamino-phenyl)-6-hydroxy-benzothiazole ([ $^{11}\text{C}$ ]6-OH-BTA-1)]. *J Labelled Compds Radiopharm*. 2004;47:679–682.
- Browne JA. A row-action alternative to the EM algorithm for maximising likelihood in emission tomography. *IEEE Trans Med Imaging*. 1996;15:687–699.
- Logan J, Fowler JS, Volkow ND, Wang GJ, Ding YS, Alexoff DL. Distribution volume ratios without blood sampling from graphical analysis of PET data. *J Cereb Blood Flow Metab*. 1996;16:834–840.
- Small GW, Kepe V, Ercoli LM, et al. PET of brain amyloid and tau in mild cognitive impairment. *N Engl J Med*. 2006;355:2652–2663.
- Braak H, Braak E. Frequency of stages of Alzheimer-related lesions in different age categories. *Neurobiol Aging*. 1997;18:351–357.
- Thal DR, Rub U, Orantes M, Braak H. Phases of A beta-deposition in the human brain and its relevance for the development of AD. *Neurology*. 2002;58:1791–1800.
- Arnold SE, Hyman BT, Flory J, Damasio AR, Van Hoesen GW. The topographical and neuroanatomical distribution of neurofibrillary tangles and neuritic plaques in the cerebral cortex of patients with Alzheimer's disease. *Cereb Cortex*. 1991;1:103–116.
- Minoshima S, Giordani B, Berent S, Frey KA, Foster NL, Kuhl DE. Metabolic reduction in the posterior cingulate cortex in very early Alzheimer's disease. *Ann Neurol*. 1997;42:85–94.
- Ishii K, Sasaki M, Matsui M, et al. A diagnostic method for suspected Alzheimer's disease using  $\text{H}_2^{15}\text{O}$  positron emission tomography perfusion Z score. *Neuroradiology*. 2000;42:787–794.
- Nyback H, Nyman H, Blomqvist G, Sjogren I, Stone-Elander S. Brain metabolism in Alzheimer's dementia: studies of  $^{11}\text{C}$ -deoxyglucose accumulation, CSF monoamine metabolites and neuropsychological test performance in patients and healthy subjects. *J Neurol Neurosurg Psychiatry*. 1991;54:672–678.
- Cutler NR, Haxby JV, Duara R, et al. Clinical history, brain metabolism, and neuropsychological function in Alzheimer's disease. *Ann Neurol*. 1985;18:298–309.
- Ishii K, Sasaki M, Kitagaki H, et al. Reduction of cerebellar glucose metabolism in advanced Alzheimer's disease. *J Nucl Med*. 1997;38:925–928.
- Ishii K, Kono AK, Sasaki H, et al. Fully automatic diagnostic system for early- and late-onset mild Alzheimer's disease using FDG PET and 3D-SSP. *Eur J Nucl Med Mol Imaging*. 2006;33:575–583.
- Mosconi L, Herholz K, Prohovnik I, et al. Metabolic interaction between ApoE genotype and onset age in Alzheimer's disease: implications for brain reserve. *J Neurol Neurosurg Psychiatry*. 2005;76:15–23.
- Price JL, Morris JC. Tangles and plaques in nondemented aging and "preclinical" Alzheimer's disease. *Ann Neurol*. 1999;45:358–368.
- Bennett DA, Schneider JA, Arvanitakis Z, et al. Neuropathology of older persons without cognitive impairment from two community-based studies. *Neurology*. 2006;66:1837–1844.
- Mintun MA, Larossa GN, Sheline YI, et al. [ $^{11}\text{C}$ ]PIB in a nondemented population: potential antecedent marker of Alzheimer disease. *Neurology*. 2006;67:446–452.